Line-spacing Multiplied Optical Frequency Combs Generation using an Electro-Optic Talbot Laser and Cross-Phase Modulation in a Fiber

Juanjuan Yan *, Haiyan Dong , Yu Wang

Posted Date: 1 March 2024

doi: 10.20944/preprints202403.0020.v1

Keywords: Optical frequency comb; electro-optic Talbot laser; cross-phase modulation; line-spacing multiplication

Article

Line-Spacing Multiplied Optical Frequency Combs Generation Using an Electro-Optic Talbot Laser and Cross-Phase Modulation in a Fiber

Juanjuan Yan *, Haiyan Dong and Yu Wang

School of electronic information engineering, Beihang University, Beijing 100191, China
* Correspondence: yanjuanjuan@buaa.edu.cn

Abstract: An optical frequency comb (OFC) generator based on an electro-optic Talbot laser and cross-phase modulation (XPM) in a high nonlinear fiber (HNLF) is designed and demonstrated. The Talbot laser is an electro-optic frequency shifting loop to produce repetition rate multiplied pulses, and these pulses working as a pump signal induce XPM process in the HNLF to modulate the phase of a probe signal. At the output of the HNLF, OFCs with a multiplied line-spacing can be generated. The effects of the pump power and the HNLF length on the performance of the generated OFCs are theoretically analyzed. In the experiments, the line-spacing of the generated OFCs is respectively multiplied to be 10 GHz, 15 GHz and 20 GHz with a factor of 2, 3 and 4. The center of the OFCs is tuned in a 4-nm range by adjusting the wavelength of the probe signal.

Keywords: optical frequency comb; electro-optic Talbot laser; cross-phase modulation; line-spacing multiplication

1. Introduction

Optical frequency combs (OFCs) can be used in many applications such as arbitrary waveform generation (AWG) [1], wave division multiplexed systems [2], frequency measurements [3] and so on [4]. Mode-locked lasers (MLLs) have been earliest employed for the OFC generation [5]. However, the line-spacing of the generated OFC is on the order of tens of MHz determined by the cavity length of the MLL. Some solutions have been put forward to produce OFCs with a spacing on the order of GHz, including harmonic mode-locking [6], micro-resonator [7], electro-optic modulation of a continuous wave (CW) laser [8] and Talbot effects based method [9]. The last approach has attracted more attention owing to its advantages of flexibility. In this method, the pulse repetition rate of a lower-rate laser source is multiplied via temporal Talbot effect also referred to as temporal self-imaging by launching the pulse laser into a dispersive medium, and then the repetition rate multiplied pulses as pump signals are co-coupled into a length of high nonlinear fiber (HNLF) with a CW probe [9,10]. In this way, cross-phase modulation (XPM) process is induced in the HNLF, and the resulted OFC has a line-spacing equal to the multiplied repetition rate of the pump pulses. Dispersive fibers [11] or linearly chirped fiber Bragg gratings (LCFBG) [12] can be applied to achieve pulse repetition rate multiplication (PRRM).

In [9], MLL pluses at a 250-MHz repetition are used and PRRM is realized through temporal Talbot effects in a dispersion compensation fiber (DCF). A multiplication factor up to 1540 is achieved, and the resulted OFC has a frequency spacing of 385 GHz. However, due to the low repetition rate of the original pulses, a long fiber is required to satisfy the Talbot condition. Also the third-order dispersion in the DCF results in the distortion of the output pulses and additional peaks around each spectral line of the generated comb [9]. To obtain a pulse train at a rate of 10 GHz, pulse compression and reshaping are applied to the generated waveform by intensity and phase modulation of a CW light in [10]. And the rate of the pulses is then multiplied with a factor of 5 via temporal Talbot effect in a combined dispersive fiber consisting of 0.54 km simple single mode fiber and 3.02 km DCF. Similarly, the 50-GHz pulse train and a CW probe are coupled into a HNLF to

 doi:10.20944/preprints202403.0020.v1

induce XPM process, and an OFC with a line-spacing of 50 GHz is produced [10]. In the scheme, two relatively short dispersive fibers are used to provide a total dispersion for the realization of the pulse rate multiplication. A propagation loss is also inevitably introduced. A LCFBG can be employed to reduce this loss [9]. However, the advances in grating fabrication, especially in terms of repeatability, are required to achieve tunable PRRM [12].

A Talbot laser is an alternative method for the pulse repetition rate multiplication. The traditional Talbot laser is a frequency shifted feedback laser based on an acoustic optic frequency shifter, and the working frequency is usually tens of MHz [13]. While an electro-optic (EO) frequency shifter is applied, a GHz Talbot laser can be achieved [14]. Here, we design and demonstrate a line-spacing multiplied OFC generator by a combined use of an EO Talbot laser and XPM in a HNLF, avoiding the needs of MLLs and long dispersive fibers. In the EO Talbot laser, the frequency shifter is realized with a dual-parallel Mach-Zehnder modulator (DPMZM). The working principle of this OFC generator is theoretically modeled and the influences of pump power and the length of the HNLF on the performance of the generated OFC are analyzed. In the experiments, the DPMZM is driven by a 5-GHz radio frequency (RF) signal, and optical pulses with a repetition rate of 10 GHz, 15 GHz and 20 GHz are respectively produced with the EO Talbot laser. Correspondingly, OFCs with a line-spacing of 10 GHz, 15 GHz and 20 GHz are generated after XPM process in a 200-m HNLF. The comb line-spacing is respectively multiplied with a factor of 2, 3 and 4. The wavelength tunability of the generated OFCs is also demonstrated in a range of 4 nm.

2. Principles

The schematic diagram of the proposed system for generating a line-spacing multiplied OFC is shown in Figure 1. This OFC generator consists of an EO Talbot laser loop and a length of HNLF. The light from a CW laser is injected into the frequency shifting loop via a 2×2 optical coupler (OC1), and a polarization controller (PC1) is used to adjust the polarization state of the light so as to obtain a maximum transmission efficiency. In the loop, the light is sent to a DPMZM and carrier-suppression single sideband (CS-SSB) modulated by a RF signal at a frequency of f_s. In this way, a frequency shift of f_s is achieved. The modulated laser is then amplified with an Erbium-doped fiber amplifier (EDFA1) in order to compensate for the losses in the loop, and an optical bandpass filter (OBPF1) is employed to filter out the amplified spontaneous emission (ASE) noise generated by EDFA1. A tunable delay line (TDL) is inserted before OC1 to adjust the delay time of the loop, τ_c.

To perform CS-SSB modulation, the two sub-modulators (MZM-a and MZM-b) of the DPMZM are biased at the minimum transmission point, and the main modulator (MZM-c) is at the quadrature transmission point. The signal from the RF source is divided equally into two branches to drive the two sub-modulators with a phase difference of 90 degrees. In this case, the output field of the DPMZM is expressed as

$$E_{DPMZM}(t)=\sqrt{2P_{in}}\exp(j2\pi f_0 t)\left[\sin\left(\frac{\pi V_m\cos(2\pi f_s t)}{V_\pi}\right)+j\sin\left(\frac{\pi V_m\sin(2\pi f_s t)}{V_\pi}\right)\right] \quad (1)$$

where P_{in} and f_0 are respectively the average power and frequency of the input optical field to the modulator, V_m is the amplitude of the modulation signal, and V_π is the half-wave voltage of the two sub-modulators. In the case of small signal modulation, the higher-order sidebands are ignored, and the CS-SSB modulated optical field is written as

 doi:10.20944/preprints202403.0020.v1

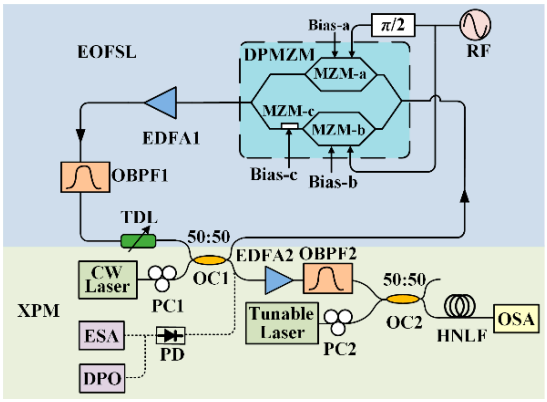

Figure 1. Schematic diagram of OFC generation with a multiplied spectral line-spacing. (CW Laser: continuous wave laser; PC: Polarization controller; OC: Optical coupler; RF: radio frequency; DPMZM: Dual parallel Mach-Zehnder modulator; EDFA: Erbium doped fiber amplifier; OBPF: Optical band pass filter; TDL: Tunable delay line; HNLF: highly nonlinear fiber, PD: Photo-detector; ESA: electrical signal analyzer; DPO: Digital phosphor oscilloscope; OSA: Optical spectrum analyzer).

$$E_{DPMZM}(t) \approx \sqrt{2P_{in}} J_1(\pi\beta) \exp[j2\pi(f_o + f_s)t] \tag{2}$$

where J_1 is the first-order Bessel function of the first kind, $\beta=V_m/V_\pi$ is the modulation depth. From Eq. (1), it is clear that the frequency of the light is shifted by the RF frequency f_s in each roundtrip. Thus, the resulting field at the output is a comb of optical frequencies separated by f_s, and it is expressed as

$$E_{out}(t) = \sqrt{2P_{in}} \exp(j2\pi f_o t) \times \sum_{k\geq 0} J_1^k(\pi\beta) \left(\sqrt{\alpha_o g}\right)^k \exp\left(-j2\pi k\left(f_s t - f_o \tau_c\right)\right) \exp\left(j\pi k(k+1)\frac{f_s}{f_c}\right) \tag{3}$$

where g represents the power gain provided by EDFA1, α_o is the insertion loss of the loop and $f_c=1/\tau_c$ is the free spectral range. When $f_s/f_c=p/q$ (p and q being coprime integers), the pulse repetition rate becomes qf_s. In this case, temporal Talbot effect is induced. The process results in the pulse repetition rate being multiplied to q times of the original. However, the frequency spacing of the OFC expressed by Eq. (3) remains to be f_s. To achieve the spacing multiplication, the effect of XPM in the HNLF is employed here.

As shown in Figure 1, the output pulses of the frequency shifting loop are amplified with EDFA2 and injected into another OBPF2 to filter out the ASE noise. Then the output signals are coupled into a section of HNLF as the pump to induce XPM effect. The probe signal is a CW from a tunable laser at a frequency of ω_{pb}. After the XPM process, the optical field of the probe signal can be expressed as

$$E_{pb}(t) \propto \exp(j\omega_{pb}t) \exp[j\phi_{NL}(t)] = \exp(j\omega_{pb}t) \exp[jm_{XPM} P_{pump}(t)] \tag{4}$$

where $\varphi_{NL}(t)$ is the nonlinear phase shift introduced to the probe signal, $P_{pump}(t)$ is the instantaneous power of the pump, and m_{XPM} is a complex number determined by the nonlinear coefficient, the length of the HNLF and propagation loss as well as the relative state of polarization between the pump and probe [15]. Here, another PC (PC2) is used to align the polarization states of the pump and the probe. In this case, when the propagation loss, dispersion and birefringence in the HNLF are negligible, $\varphi_{NL}(t)$ is related to the pump power by [16]

$$\varphi_{NL}(t) = 2\gamma L_{HNLF} P_{pump}(t) = 2\gamma L_{HNLF} G T_f |E_{out}(t)|^2 \tag{5}$$

where γ and L_{HNLF} are respectively the nonlinear coefficient and the length of the HNLF, G is the power gain provided by EDFA2, T_f is the power loss introduced by OBPF2, and $E_{out}(t)$ is the output field of the Talbot laser described as Eq.(3). According to Eq.(4), the corresponding optical spectrum of the probe signal is written as

 doi:10.20944/preprints202403.0020.v1

$$F_{pb}(\omega)\infty\left|\int_{-\infty}^{+\infty}\exp\left[jm_{XPM}P_{pump}(t)\right]\exp\left[-j(\omega-\omega_{pb})t\right]dt\right|^2$$
$$\approx\left|\int_{-\infty}^{+\infty}\left[1+m_{XPM}P_{pump}(t)\right]\exp\left[-j(\omega-\omega_{pb})t\right]dt\right|^2=\delta(\omega-\omega_{pb})+m_{XPM}^2\cdot S_{RF}(\omega-\omega_{pb}) \quad (6)$$

where Taylor expansion of the exponential function is applied and it is simplified for weaker XPM ($m_{XPM}\cdot P_{pump}(t)$<<1 radian). $S_{RF}(\omega)$ is the RF spectrum of the pump pulses. Therefore, the optical spectrum of the probe after XPM is proportional to the RF spectrum of the pump superimposed on the Dirac delta function, $\delta(\omega)$. If the pump is pulses with a repetition rate of qf_s, the corresponding RF spectrum consists of frequency lines spaced at qf_s, and the optical spectrum of the probe becomes an OFC with a line-spacing of qf_s. From Eq. (3), it is known that the pulse repetition rate can be multiplied to be qf_s when the delay time of the frequency shifting loop is adjusted to meet the condition of $f_s/f_c=p/q$ (p and q being coprime integers). So the comb line-spacing multiplication can be achieved by tuning the TDL in the loop.

To confirm the principle described above, some simulations are firstly performed. In the simulations, the DPMZM is modeled as Eq.(1), and the frequency of the RF signal is f_s=5 GHz. The wavelength of the pump laser and the signal laser is respectively 1550nm 和 1553.1nm. The dispersion coefficient and dispersion slope of the HNLF are respectively -2.569ps/nm/km and 0.005ps/nm^2/km @1550nm. The attenuation coefficient and nonlinear coefficient are 1.5 dB/km and 11W^{-1}km^{-1}, respectively. The nonlinear process of XPM in the HNLF is simulated by numerically solving the nonlinear Schrödinger equations using the split-step Fourier method [15]. With p=1, and q=2, 3, 4 respectively, the pump pluses from the EO Talbot laser are presented in Figure 2a. It is clear that the pulse repetition rate is respectively 10 GHz, 15 GHz and 20 GHz, i.e., PRRM with a factor of 2, 3 and 4 is realized. The corresponding RF power spectra of these pulses are shown in Figure 2b. When the length of the HNLF is L_{HNLF}=200m and the average pump power injected into the HNLF is P_{av_pump}=14 dBm, the resulted OFCs are shown in Figure 2c, and they are centered at the probe wavelength. By comparing Figure 2b,c, it can be found that the line-spacing of the two spectra for a given q is equal to qf_s, and the envelope of an OFC spectrum is approximately the superposition of a RF spectrum envelope and the probe spectral line, as concluded from Eq.(6).

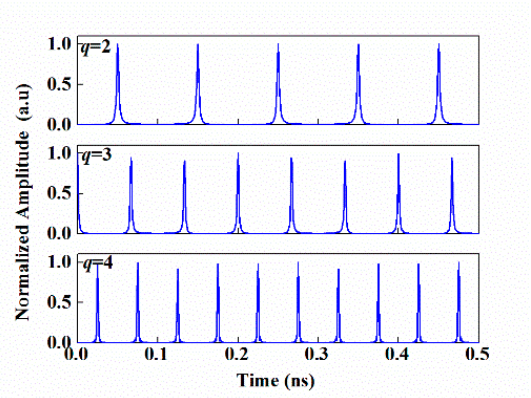

(**a**)

Preprints.org (www.preprints.org) | NOT PEER-REVIEWED | Posted: 1 March 2024 doi:10.20944/preprints202403.0020.v1

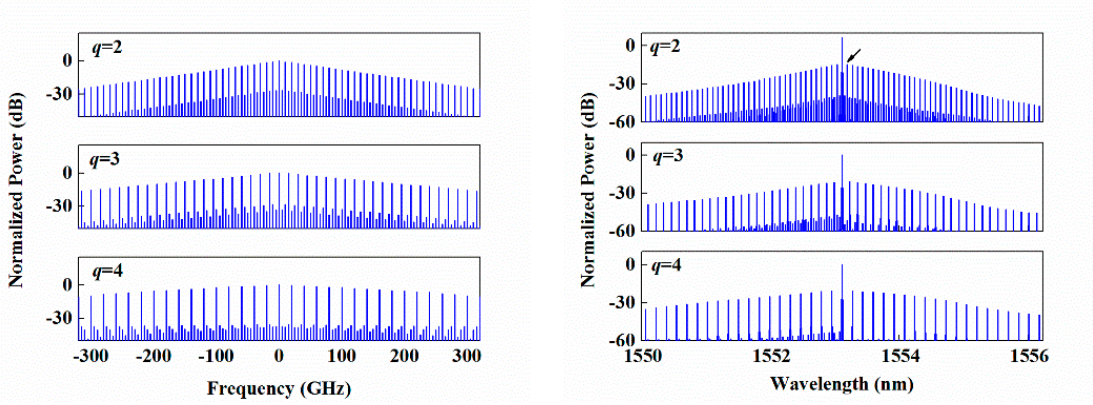

Figure 2. The simulated results with p=1 and q=2, 3, 4 respectively, (a) pump pulses output from the EO Talbot laser, (b) the RF power spectra of the pulses in (a) and (c) the produced OFCs at the output of the HNLF.

In our study, the right comb line nearest to the probe spectral line pointed by the arrow in Figure 2c with q=2 is taken as an example to investigate the influences of the HNLF parameters on the performance of the generated OFCs, and the side-mode suppression ratio (SMSR) and peak power of this line are taken into account. The results are shown in Figure 3a with L_{HNLF}=200m. It can be seen that the SMSR is increasing and then decreasing with the increase of the pump power, while the peak of the line keeps increasing in these considered cases. When P_{av_pump} is set to be 6dBm, the SMSR has a peak value about 26.5dB. In this case, the line-spacing doubled OFC is presented in Figure 3b, where those OFCs with P_{av_pump}=14dBm and 22dBm are also shown as a comparison. From Figure 3b, it is also clear that more lines are generated in the range of 6 nm due to the fact that the higher the pump power and the stronger the XPM nonlinearity. However, the SMSR of each line is decreased for the simultaneously enhanced four wave mixing (FWM) interactions among all the modes [15]. Also Eq.(6) is not applicable since the nonlinear phase induced by XPM becomes larger. For the case of P_{av_pump}=22dBm in Figure 3b, the nonlinear phase is $\varphi_{NL}=2\gamma L_{HNLF}P_{av\_pump} \approx 0.7$ radian. Consequently, the envelop of the resulting OFC cannot be regarded as a superposition of the RF spectrum of the pump and the probe spectral line. As a compromise, the pump power P_{av_pump} is set to be 14dBm in the following.

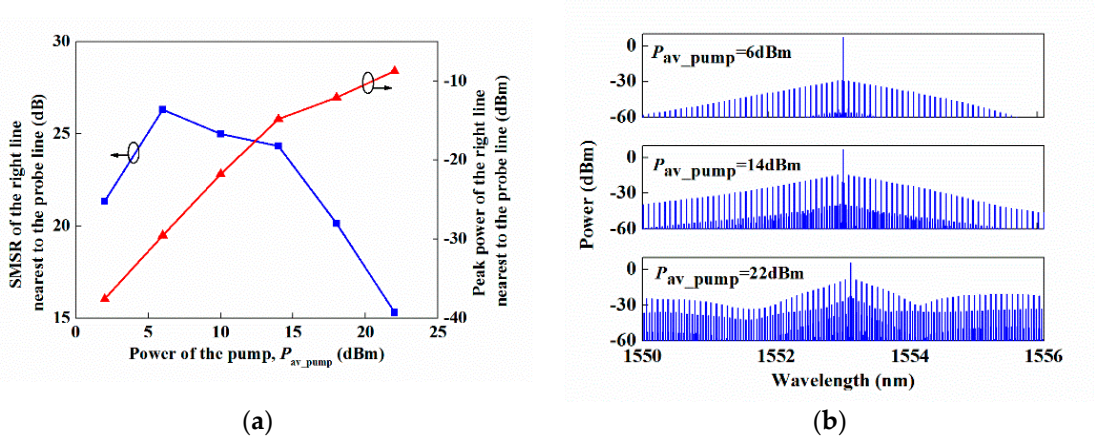

Figure 3. The simulated results with p=1 and q=2, (a) the SMSR and the peak power of the right line nearest to the probe line as a function of the pump power injected into the HNLF and (b) the generated OFCs respectively with P_{av_pump}=6dBm, 14dBm and 22dBm.

Similarly, the SMSR and peak power of the considered line are respectively shown in Figure 4a as a function of the HNLF length, L_{HNLF}. It can be observed that the SMSR is also increasing and then

 doi:10.20944/preprints202403.0020.v1

decreasing with L_{HNLF} increased while the peak of the line keeps increasing in all the considered cases. When L_{HNLF} is 100m, the SMSR has a peak value about 26dB. Figure 4b shows the resulted OFCs with L_{HNLF}=100m, 200m, and 600m. It can also be found that more comb lines are generated with the length of the HNLF increased since the XPM nonlinearity is accumulated along the HNLF. However, the SMSR is decreased with L_{HNLF} > 100m also mainly due to the enhanced FWM efficiency. As a compromise of the SMSR and the bandwidth, a 200-m HNLF is applied in our experiments.

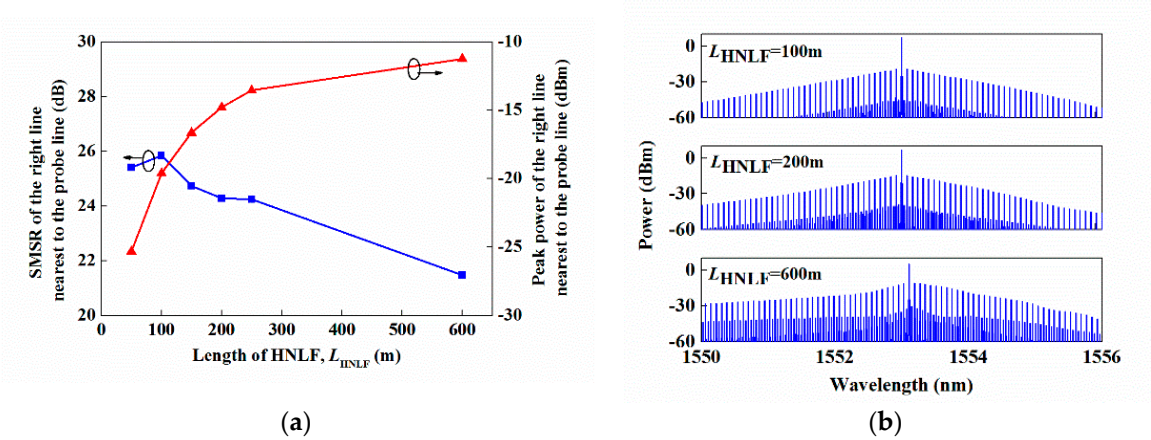

Figure 4. The simulated results with p=1 and q=2, (a) the SMSR and the peak power of the right line nearest to the probe line as a function of the HNLF length and (b) the generated OFCs respectively with L_{HNLF}=100m, 200m and 600m.

3. Experimental Results

The proving experiments on the system in Figure 1 are also performed. A CW laser (RIO Orion laser module) working at 1549.76 nm is employed, and the output power is 9 dBm. The used DPMZM (Thorlab LN86S-FC) has a bandwidth of 14 GHz, and the half-wave voltages of the two sub-MZMs and the main modulator are respectively 4.5V and 6V. The modulator is driven by a 5-GHz RF signal to perform CS-SSB modulation. A home-built EDFA1 is applied to provide an optical gain of 18 dB. The bandwidth of the OBPF1 is about 7 nm with a center of 1550 nm. The tunable range of the used TDL (GP-UM-MDL-002) is 0~330ps. The length of the EO Talbot laser loop is about 25.5 m, and the roundtrip delay is calculated to be about 124.1 ns with the refractive index of the fiber core equal to 1.46. The optical pulses after frequency multiplication are detected by a PD and observed with a digital phosphor oscilloscope (DPO, Tektronix DPO72004). The responsivity of the PD is 0.55 A/W, and the bandwidth is 30GHz. The pump pulses from the Talbot laser are amplified and then passing through OBPF2 (Finisar WaveShaper 1000S) with a bandwidth of 1.6 nm. The probe light is from a tunable CW laser (Optilab TWL-C-M), and the power is 6dBm. The length of the used HNLF is 200m. The dispersion coefficient and dispersion slope of the fiber are respectively -2.569ps/nm/km and 0.005ps/nm^2/km at 1550nm. The nonlinear coefficient is measured to be 10.7 W^{-1}km^{-1} with the method based on measurement of the self-phase modulation effect induced nonlinear phase shift [17]. The optical spectra obtained in the experiments are monitored by the OSA (YOKOGAWA AQ6370C).

Figure 5a shows the output spectrum of the DPMZM when the loop is not closed, and it is clear that CS-SSB modulation is realized with -1st order sideband remained. The side-mode suppression ratio is measured to be 18.5dB. When the loop is closed, the generated OFC is presented in Figure 5b. As expected, the new generated spectral lines lie in the region of longer wavelength. The net gain of the loop is less than unity to obtain a stable spectrum [18]. As a result, the intensity of the new generated line is gradually decreasing. The line spacing of the OFC is 0.04 nm corresponding to 5 GHz at the wavelength of 1550nm. At the same time, the observed pulse train is shown in Figure 5c, and the period of the pulses is 0.2 ns.

 doi:10.20944/preprints202403.0020.v1

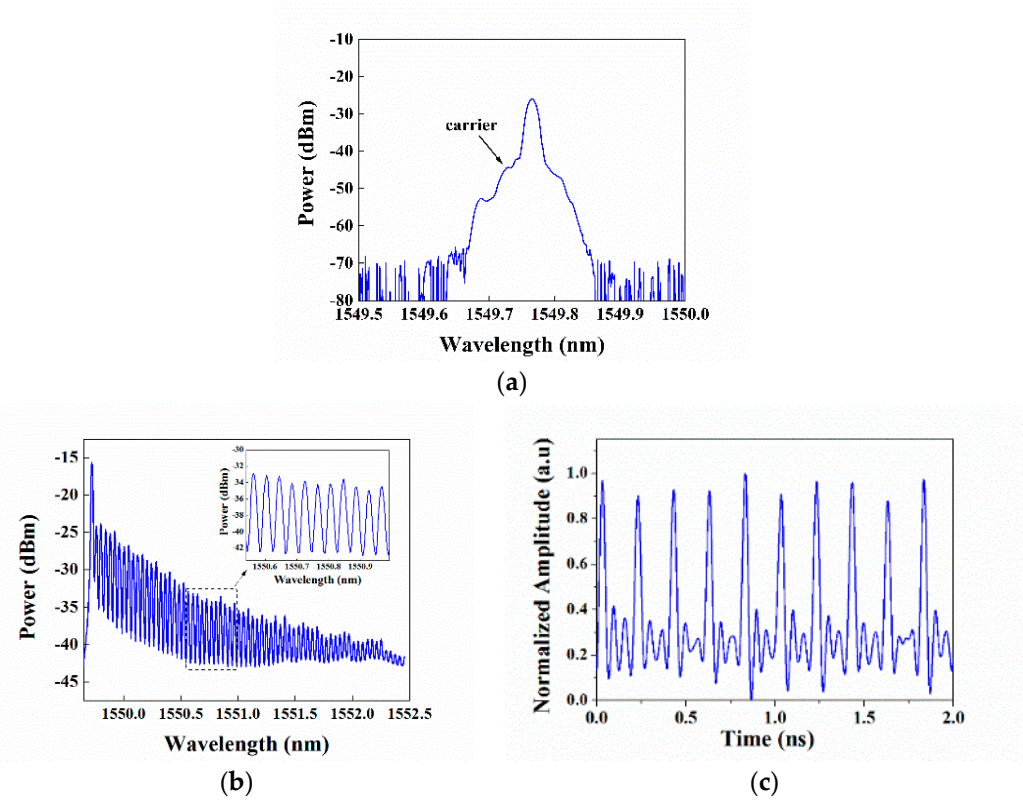

Figure 5. Experiments results, (a) the output spectrum of the DPMZM with CS-SSB modulation achieved (b) the generated OFC and (c) pules at the output of the loop.

In the experiments, the TDL is adjusted to change the ratio of f_s/f_c so as to induce temporal Talbot effects. When the time delay is set to be 0ps, 34ps and 51ps, the corresponding Talbot effects with $f_s/f_c=p/q$=1241/2, 1862/3 and 2483/4 are respectively realized. The output pulses are shown in Figure 6a. The repetition frequencies of the pulses are respectively 10 GHz, 15 GHz and 20 GHz, i.e. they are 2 times, 3 times and 4 times of the repetition rate of the original pulses. It is clear that the amplitude fluctuations become more obvious with the multiplication factor increasing. Some facts lead to this phenomenon. Firstly, the fluctuations are mainly resulted from the noise introduced by the EDFA1, the laser, the RF source and the PD. Secondly, the bandwidth of the generated OFC in Figure 5b is limited. Consequently the pulses are not narrow enough, which results in pulse overlapping with the increase of the multiplication factor. Finally, the observed results are also affected by the limited 20-GHz bandwidth of our used DPO. The corresponding RF power spectra of these pulses are presented in Figure 6b. It can be seen that 5-GHz and 15-GHz tones are suppressed with a ratio about 20dB against other harmonics of 10 GHz and 20 GHz with $f_s/f_c=p/q$=1241/2, indicating a pulse repetition multiplication of 2 is well achieved. However, the harmonics suppression ratio is decreased for the other two cases in Figure 6b, which also reveals a degraded pulse rate multiplication. This can be improved by optimizing the power and the net gain in the loop so as to increase the bandwidth of the generated OFC. Here, the OFC spectrum output from the EO Talbot laser is unchanged while the pulse rate is multiplied. To make the comb line-spacing multiplied, after further amplifying and filtering the pump pulses are coupled into the HNLF with the 1553.1-nm probe CW from the tunable laser. When the pump power injected into the HNLF is 14dBm, the corresponding probe spectra at the output of the HNLF are shown in Figure 6c. It can be found that the line-spacing of the OFC is respectively multiplied to be 0.08 nm, 0.12 nm and 0.16 nm, i.e.10 GHz, 15 GHz and 20 GHz when the pump pulse rate multiplication factor is 2, 3 and 4, respectively. So owing to the XPM process, OFCs with line-spacing multiplied by a factor of 2, 3 and 4 are generated.

Preprints.org (www.preprints.org) | NOT PEER-REVIEWED | Posted: 1 March 2024 doi:10.20944/preprints202403.0020.v1

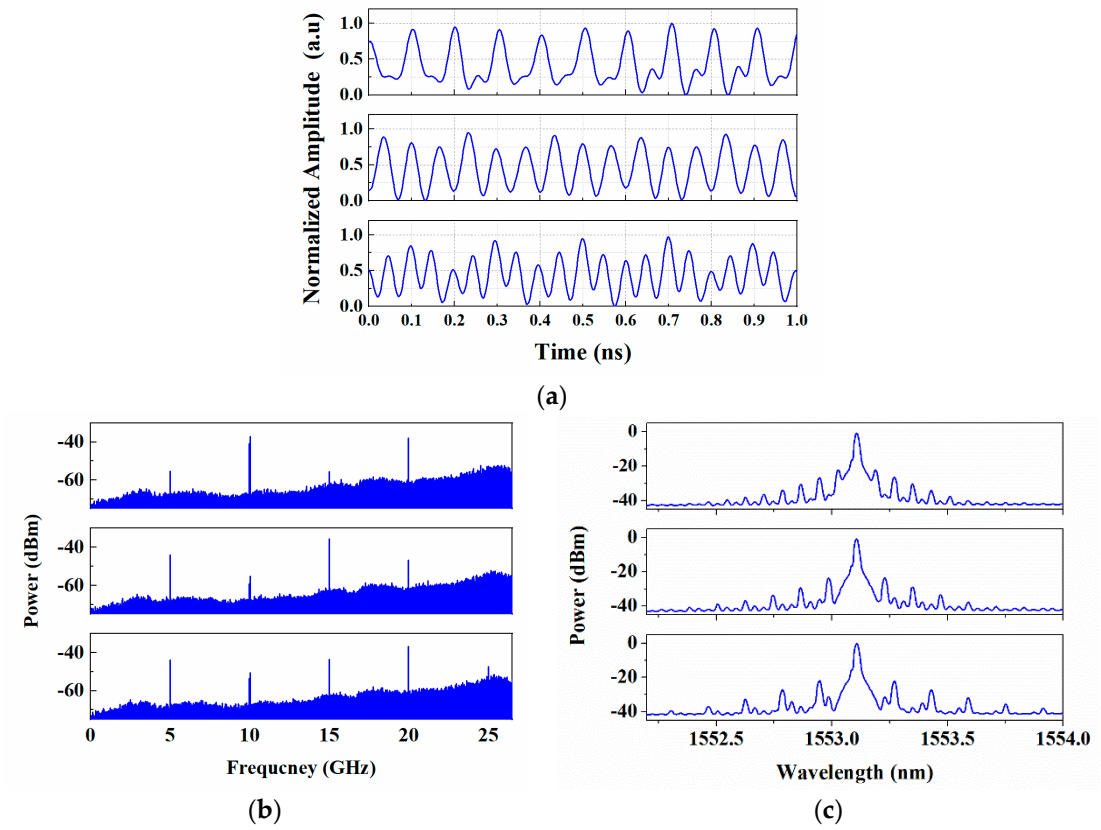

Figure 6. Experimental results with p/q=1241/2, 1862/3 and 2483/4 respectively, (a) the generated pump pulses from the EO Talbot laser, (b) the corresponding RF power spectra of the pulses in (a) and the spectra of the probe light at the output of the HNLF.

As shown in Figure 6c, the center of the output OFC is determined by the working wavelength of the probe light. So this scheme is also wavelength tunable. In our experiments, the wavelength of the probe signal is tuned from 1553nm to 1557nm. The generated OFCs respectively at the center wavelength of 1553.1nm, 1554.7nm and 1556.3nm are presented in Figure 7 with $f_s/f_c=p/q$=1241/2 and a pump power of 22 dBm. From this figure, it can be seen that the OFC spectral envelope shapes centered at different wavelength are similar. Compared with the spectrum in Figure 6c, the power of each frequency line is increased since the XPM process is enhanced by the increased pump power. And the spectra become asymmetrical around the center wavelength, which is resulted from the chirps of the pump pulses. This conclusion can also be drawn from Figure 3b with P_{av_pump}=22dBm.

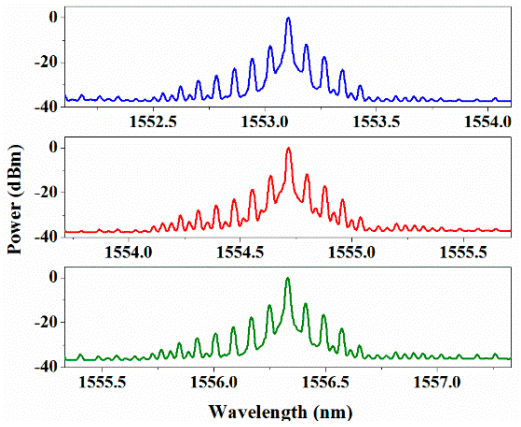

Figure 7. The probe spectra at the output of the HNLF with $f_s/f_c=p/q$=1241/2 and the CW probe at the wavelength of 1553.1nm, 1554.7nm and 1556.3nm, respectively.

 doi:10.20944/preprints202403.0020.v1

4. Discussion

From the above theoretical and experimental results, it is clear that OFC line-spacing multiplication can be achieved using our scheme. The multiplication factor is tuned by adjusting the TDL in the EO Talbot laser loop. Compared with the existing methods in [9,10], our method avoids the use of MLLs and long dispersive fibers. The bandwidth of the generated OFC is also determined by the bandwidth and power of the pump from the laser loop except the length and the nonlinear coefficient of the HNLF. More comb lines can be experimentally generated in the Talbot laser by increasing the net gain and optimizing the power in the loop, which contributes to generate pump pulses with a narrow width and a larger peak power. In this way, the line-spacing multiplication factor and the bandwidth of the resulting OFC can be increased.

Finally, it should be pointed out that the product of the nonlinear coefficient and the length of the used HNLF also needs to be optimized to further improve the SMSR performance of the line-spacing multiplied OFC, for the FWM effect also exists in the HNLF. A section of HNLF with a small dispersion is required to decreasing the FWM efficiency.

5. Conclusions

A scheme for the generation of line-spacing multiplied OFCs is proposed and demonstrated. This OFCs generator is composed of an EO Talbot laser and a length of HNLF. The frequency shifter in the Talbot laser is a DPMZM performing CS-SSB modulation. The pulses output from the Talbot laser work as pumps to stimulate XPM process in the HNLF. By adjusting the TDL in the Talbot laser loop, the repetition rate of the pump pulses can be multiplied, and the line-spacing of the generated OFCs at the output of the HNLF is correspondingly multiplied with a same factor. The principle of this OFCs generator is theoretically modeled and simulated to investigate the influences of the pump power and HNLF length on the performance of the generated OFCs. In the experiments, the DPMZM is driven by a 5-GHz RF signal. OFCs with a line spacing of 10 GHz, 15 GHz and 20 GHz are respectively produced with a multiplication factor of 2, 3 and 4. If the optical power and the net gain in the Talbot laser loop is optimized, the bandwidth of the generated OFC can be increased, and a greater multiplication factor can be realized. The center of the generated OFCs is determined by the wavelength of the probe light, and it can be tuned while keeping a similar spectral envelop. So this scheme has the advantage of wavelength tunability with no needs of MLLs and long dispersive fibers. It can be applied in the optical arbitrary waveform generation and wave division multiplexed systems.

Author Contributions: Conceptualization, J. Yan; methodology, J. Yan; software, H. Dong and Y. Wang; validation, J. Yan; investigation, H. Dong and J. Yan; data curation, H. Dong and Y. Wang; writing—original draft preparation, H. Dong and J. Yan; writing—review and editing, J. Yan.; visualization, H. Dong; supervision, J. Yan; funding acquisition, J Yan. All authors have read and agreed to the published version of the manuscript.

Funding: This research was supported by the National Natural Science Foundation of China (NSFC) (61771029, 61201155).

Data Availability Statement: Data underlying the results presented in this paper are not publicly available but may be obtained from the authors upon reasonable request

Conflicts of Interest: The authors declare no conflict of interest.

References

1. Huang, C. B.; Jiang, Z.; Leaird, D. E.; Caraquitena, J.; Weiner, A. M. Spectral line-by-line shaping for optical and microwave arbitrary waveform generations. *Laser & Photon. Rev.* **2008**, *2*, 227–248. doi: 10.1002/lpor.200810001.
2. Hraghi, A.; Chaibi, M. E.; Menif, M.; Erasme, D. Demonstration of 16QAM-OFDM UDWDM Transmission Using a Tunable Optical Flat Comb Source. *J. Lightwave Technol.* **2017**, *35*, 238–245. doi: 10.1109/JLT.2016.2636442.

3. Shen, J.; Wu, S.; Li, D.; Liu, J. Microwave multi-frequency measurement based on an optical frequency comb and a photonic channelized receiver. *Appl. Opt*. **2019**, *58*, 8101-8107. doi: 10.1364/AO.58.008101.
4. Fortier, T.; Baumann, E. 20 years of developments in optical frequency comb technology and applications. *Commun. Phys*. **2019**, *2*, 1-16. doi: 10.1038/s42005-019-0249-y.
5. Diddams, S. A. The evolving optical frequency comb [Invited]. *J. Opt. Soc. Am. B*. **2010**, *27*, B51. doi: 10.1364/JOSAB.27.000B51.
6. Nielsen, L.; Heck, M. J. R. Fully integrated 45-GHz harmonically mode-locked ring laser with an intra-cavity Mach–Zehnder filter. *Opt. Lett*. **2021**, 46, 880-883. doi: 10.1364/OL.415356.
7. Kippenberg, T. J.; Holzwarth, R.; Diddams, S. A. Microresonator-based optical frequency combs. *Science* **2011**, *332*, 555–559. doi: 10.1126/science.1193968.
8. Wu, R.; Supradeepa, V. R.; Long, C. M.; Leaird, D. E.; Weiner, A. M. Generation of very flat optical frequency combs from continuous-wave lasers using cascaded intensity and phase modulators driven by tailored radio frequency waveforms. *Opt. Lett*. **2010**, *35*, 3234-3236. doi: 10.1364/OL.35.003234.
9. Li, X. Z.; Seghilani, M.; Cortes, L. R.; Azana, J. Sub-THz optical frequency comb generation by efficient repetition-rate multiplication of a 250-MHz mode-locked laser. *IEEE J. Select. Topics Quantum Electron*. **2021**, *27*, 7601310. doi: 10.1109/JSTQE.2020.3039280.
10. Zheng, B.; Xie, Q.; Shu, C. Comb spacing multiplication enabled widely spaced flexible frequency comb generation. *J. Lightwave Technol*. **2018**, *36*, 2651–2659. doi: 10.1109/JLT.2018.2820223.
11. Maram, R.; Cortes, L. R.; Azana, J. Programmable fiber-optics pulse repetition-rate multiplier. *J. Lightwave Technol*. **2016**, *34*, 448–455. doi: 10.1109/JLT.2015.2500538.
12. Pudo, D.; Chen, L. R. Tunable passive all-optical pulse repetition rate multiplier using fiber Bragg gratings. *J. Lightwave Technol*. **2005**, *23*, 1729–1733. doi: 10.1109/JLT.2005.843840.
13. Chatellus, H. G. D.; Cortés, L. R.; Azaña, J. Arbitrary energy-preserving control of the line spacing of an optical frequency comb over six orders of magnitude through self-imaging. *Opt. Express* **2018**, *26*, 21069-21075. doi: 10.1364/OE.26.021069.
14. Wang, L.; LaRochelle, S. Talbot laser with tunable GHz repetition rate using an electro-optic frequency shifter. In Proceedings of Conference on Lasers and Electro-Optics, San Jose, California, USA, 14-19 May **2017**. doi: 10.1364/CLEO_AT.2017.JW2A.66.
15. Agrawal, G. P. *Nonlinear Fiber Optics*, 3rd ed.; Academic Press: San Diego, California, USA, 2001; pp260-270.
16. Pelusi, M.; Tan, H. N.; Trapala, K. S.; Inoue, T.; Namiki, S.; Low noise frequency combs for higher order QAM formats through cross-phase modulation of modelocked laser pulses. *IEEE J. Select. Topics Quantum Electron*. **2018**, *24*, 1101612. doi: 10.1109/JSTQE.2017.2769622.
17. Boskovic, A.; Gruner, N. L.; Levring, O. A.; Chernikov, S. V.; Taylor, J. R. Direct continuous-wave measurement of n_2 in various types of telecommunication fiber at 1.55 microm. *Opt. Lett*. **1996**, *21*, 1966-1968. doi: 10.1364/ol.21.001966.
18. Kanagaraj, N.; Djevarhidjian, L.; Duran, V.; Schnebelin, C.; Chatellus, H. G. D. Optimization of acousto-optic optical frequency combs. *Opt. Express* **2019**, *27*, 14842-14852. doi: 10.1364/OE.27.014842.